Control Strategies For Maximizing Renewable Energy Utilization In Power Systems

Michael Negnevitsky[*], Evgenii Semshchikov, James Hamilton, Xiaolin Wang , Ekaterina Bayborodina

School of Engineering, University of Tasmania, Hobart, Australia

Abstract — **Environmental and economic challenges lead to the rapid growth of the renewable energy (RE) market in many countries. At a high level of RE sources (i.e. wind and solar) penetration, power systems face technical difficulties associated with the critical frequency stability and insufficient power reserves. The problem becomes particularly acute at penetration levels higher than 50 %, when conventional generation units are forced to operate at partial load, potentially resulting in premature equipment wear. Energy storage and demand-side management may offer solutions in the future, however, at the current stage, they incorporate substantial capital investment and complicate control system. This paper suggests a control strategy for maximum RE penetration, adopting a low load diesel application integrated with a small-capacity battery energy storage system. The strategy results in improved renewable energy utilization without overcomplicating the control architecture. Initially, a mathematical model is developed, then it is validated based on an isolated power system – a power system where penetration of RE already exceeds 50 % annually. Optimized control strategies are shown to deliver a 20 % increase in renewable energy penetration in comparison to conventional ones.**

Index Terms — **Battery energy storage system, low load diesel, power system control, renewable energy.**

I. Introduction

The electrical energy generated by fossil fuel power plants contributes to the growth of greenhouse gas emissions, which, according to the Paris agreement, must be significantly decreased in the future [1]. The authorities around the world have set targets to increase the application of renewable energy sources (RES) for electricity generation. The most abundant RESs – wind and solar – are proven to be cost-effective and implemented in many existing power systems (e.g. Denmark, Ireland, and Germany) [2]. Unfortunately, these sources are stochastic and intermittent in nature, which requires more flexible power systems that, in addition to variable demand, have to deal with a variable supply [3]. With an appropriate level of the system flexibility, the balance between demand and supply can be provided at each time point. Therefore, while increasing RES penetration it is essential to take measures to improve system flexibility and to prevent future stability and reliability issues.

Demand-side management (DSM) is used in electric power systems to increase renewable energy utilization additionally improving system flexibility [3]. Such an approach is cost-efficient, however, it involves a range of different information and communications technologies (ICT), sophisticated control hierarchy and requires highly qualified personnel, which complicates the control system and increases the chances for failure.

Energy storage technology is another candidate capable to tackle the problems of RES integration and system flexibility. Energy storage systems (ESS) are generally used for energy shifting, load peak shaving, power quality regulation and provision of spinning reserve. Pumped hydroelectric power plants [4], hydrogen storage [5] and compressed air energy storage (CAES) [6] can be used in applications when the load changes slowly. Battery ESSs [7], supercapacitors [8] and superconducting magnetic energy storage (SMES) [9] respond fast and provide power quality support. The system inertia response can be improved by using flywheels [10] or implementing synthetic inertia of the battery ESS [11]. Storage is a very promising technology and is currently tested in many pilot projects, however, at this stage, it is still expensive.

Another way to sustainable RES penetration is to operate these sources flexibly – using droop controllers implemented at the power converter level [12]. De-loading of wind turbines [13] and optimized algorithms of PV
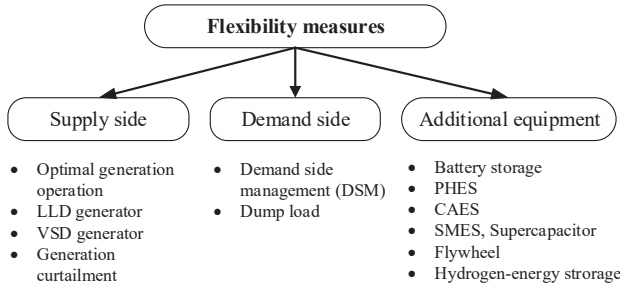
Fig. 1. Energy system flexibility measures

maximum power point tracking (MPPT) [14] are shown to improve primary frequency response. In spite of higher system flexibility, these methods result in lower RES utilization and complicated control architecture.

High RES penetration (> 60 % p.a.) has been already achieved in some Australian isolated power systems (IPS). These systems piloted technologies such as the advanced lead-acid battery, DMS, optimal generation sizing and low load diesel (LLD) generation [15]. From the experience gained through the years of the IPSs operation, one can conclude that at the current progress conventional fossil fuel generation cannot be eliminated from a power system irrespective of its size or location. With the minimization of fossil fuel energy as a target, high RES penetration can be achieved without leading to power quality or stability issues. This approach can be maximized through the use of LLD technology in combination with a low capacity battery ESS adopted in this paper. LLD allows the removal of diesel load limits (< 40% capacity constraint) resulting in greater system flexibility at high levels of RES penetration [16].

The paper is structured as follows, Section II presents different ways of RES integration. The control system architecture is outlined in Section II. The modeling methodology is given in Section IV. Case studies, shown in Section V, are based on the data from existing IPS. Section VI concludes the paper.

II. INTEGRATION OF RENEWABLE ENERGY

In traditional power systems, flexibility can be achieved by a portfolio of different kinds of power plants. Energy system flexibility can be roughly defined as an ability of a system to operate properly, ensuring the balance between generation and consumption, under uncertainty and variability in both power demand and power supply.
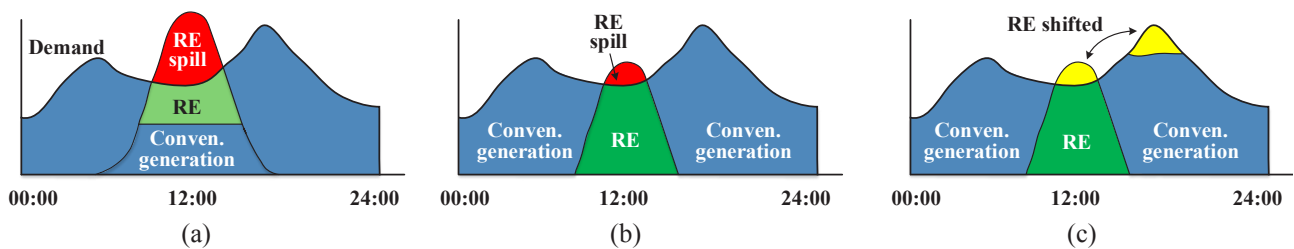
With the introduction of stochastic and intermittent electricity sources (i.e. wind and solar), the need for additional energy system flexibility increases dramatically. It can be achieved by introducing measures on the supply side, on the demand side or through placement of additional equipment such as storage technologies (Fig.1).

Due to physical constraints, a conventional generation unit operates within a specified range. By optimizing the operation of generation units, the lower load limit can be achieved. Low load and variable speed diesel engines are promising technologies capable to operate in a range from 0 to 100% loading. As a result, greater renewable energy utilization can be reached as shown in Fig. 2 (b) compared to conventional generation Fig. 2 (a). With the excess of renewable generation in the system, part of it has to be curtailed.

Demand-side management (DSM) can shift the utilization of renewable energy by reducing, increasing or re-scheduling energy demand as shown in Fig.2 (c). It can provide flexibility in terms of both power (with fast response) and energy.

The same shift in renewable energy can be performed by using storage technology. The surplus renewable energy in the grid is accumulated during favorable weather conditions and then released during the peak demand.

III. POWER SYSTEM CONTROL

With the high number of non-dispatchable renewable energy resources, the flexibility of the system can be provided by the optimally designed control system. In this context, ancillary services are of particular importance. They are used to prevent system stability and reliability issues. Depending on the involved technology (i.e. its power, energy, response capabilities), different ancillary services can be provided. Three-level control hierarchy, involving primary, secondary and tertiary control, is adopted in many conventional power systems. The timing of control ranges and associated ancillary services are presented in Fig. 3.

$$\Delta P_{dr} = K_{dr}(f - f_{ref}), \qquad (1)$$

where K_{dr} is the inverse of speed droop R:

$$R = \frac{\Delta f}{\Delta P_{dr}} = -\frac{1}{K_{dr}}. \qquad (2)$$

Frequency offset left after the primary response can be corrected by the secondary controller (or AGC – automatic generator control). It restores the primary control reserve
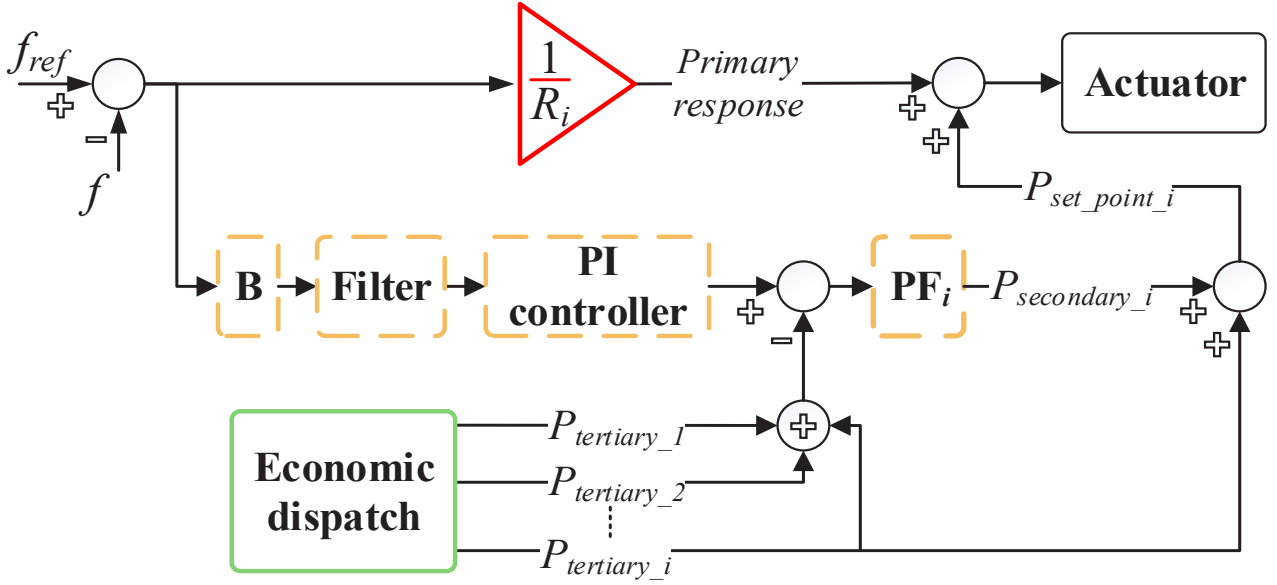

Fig. 2. Integration of RE in power systems.

Fig. 4. A general model of a governor for a controlled element.

and brings the system to its nominal operating condition. Secondary control is involved in a centralized dispatching scheme and updates operation setpoints of responsible units every 0.1 to 1 second. Secondary control is mostly implemented as a proportional-integral (PI) controller where the priority of each generating unit is determined by a participation factor. The coefficient of the PI controller and participation factor are set to represent the physical constraints of a participating unit (costs, ramp and dispatch limits). The following equation implements control action of both primary and secondary control:

$$\Delta P_d = -B \cdot G - \frac{1}{T} \int G dt, \qquad (3)$$

where P_d is the correction signal of the central regulator, $G = (f - f_{ref})$ – frequency deviation, B is a proportional term.

Tertiary control is used to restore the secondary control reserve and dispatch generation units according to the desired objective function. This function can include economic dispatch, priority dispatch, etc. Tertiary control is an automatic or manual change in operation points of all dispatchable technologies, which are updated every 1-5 minutes.

The general model of a governor at a power plant involved in all three control schemes is shown in Fig 4. It is worth noting that primary response is based on the measurements obtained locally, and secondary and tertiary controllers send updated operational setpoints via a communication network.

IV. Power system equipment modeling

A. Conventional generation

The conventional generation unit is comprised of a synchronous generator (SG) connected to the prime mover (e.g. hydraulic turbine, steam turbine, diesel engine, etc.)

controlled by the governing system (Fig.5).

The standard or seventh order model of an SG is shown in Fig. 6, in which ω_b is the base electrical angular velocity, p is a short-hand notation for the operator d/dt, T_e and T_m are electrical and mechanical torques, H is the rotor inertia, ψ_{mq} and ψ_{md} are mutual flux linkages in q-axis and d-axis. Subscripts $fd, kq1$ and $kq2$ denote one field and two damping windings.

Matrix K_s^r represents a linear transformation from stationary to rotating reference system.

A direct voltage applied to the field winding, e_{xfd} , is adjusted by the excitation system to keep the terminal voltage at its rated value. This paper adopts the IEEE AC1A excitation system.

B. Photovoltaic solar generation

A photovoltaic (PV) unit converts solar energy into DC. It is usually connected to the AC grid via DC/AC power converter as shown in Fig. 8.

PV array is a model corresponding to the single diode model that takes irradiance, ambient temperature and network voltage as input data and outputs the value of current flowing to the grid (Fig.7).

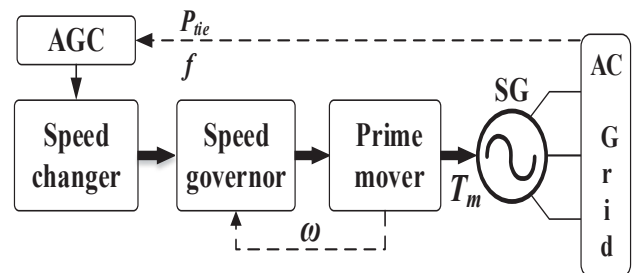The following equation is used in this paper to express PV current:
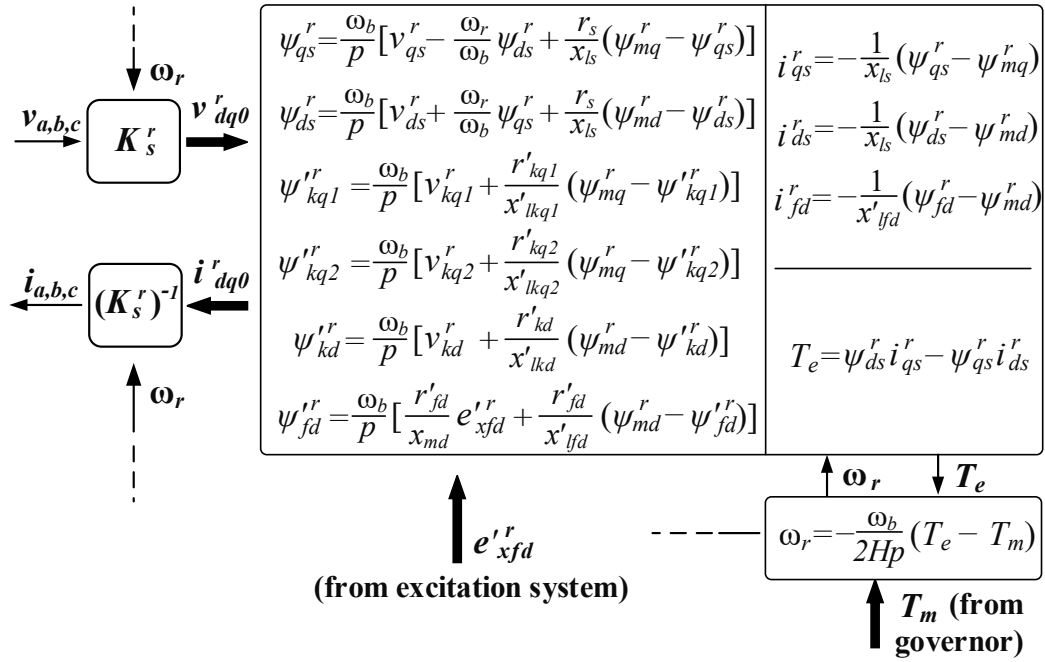

Fig. 5. Conventional generation unit.

$$\psi_{qs}^{r}=\frac{\omega_b}{p}[v_{qs}^{r}-\frac{\omega_r}{\omega_b}\psi_{ds}^{r}+\frac{r_s}{x_{ls}}(\psi_{mq}^{r}-\psi_{qs}^{r})] \qquad i_{qs}^{r}=-\frac{1}{x_{ls}}(\psi_{qs}^{r}-\psi_{mq}^{r})$$

$$\psi_{ds}^{r}=\frac{\omega_b}{p}[v_{ds}^{r}+\frac{\omega_r}{\omega_b}\psi_{qs}^{r}+\frac{r_s}{x_{ls}}(\psi_{md}^{r}-\psi_{ds}^{r})] \qquad i_{ds}^{r}=-\frac{1}{x_{ls}}(\psi_{ds}^{r}-\psi_{md}^{r})$$

$$\psi_{kq1}''^{r}=\frac{\omega_b}{p}[v_{kq1}^{r}+\frac{r'_{kq1}}{x'_{lkq1}}(\psi_{mq}^{r}-\psi_{kq1}''^{r})] \qquad i_{fd}^{r}=-\frac{1}{x'_{lfd}}(\psi_{fd}^{r}-\psi_{md}^{r})$$

$$\psi_{kq2}''^{r}=\frac{\omega_b}{p}[v_{kq2}^{r}+\frac{r'_{kq2}}{x'_{lkq2}}(\psi_{mq}^{r}-\psi_{kq2}''^{r})]$$

$$\psi_{kd}''^{r}=\frac{\omega_b}{p}[v_{kd}^{r}+\frac{r'_{kd}}{x'_{lkd}}(\psi_{md}^{r}-\psi_{kd}''^{r})] \qquad T_e=\psi_{ds}^{r}i_{qs}^{r}-\psi_{qs}^{r}i_{ds}^{r}$$

$$\psi_{fd}''^{r}=\frac{\omega_b}{p}[\frac{r'_{fd}}{x_{md}}e'^{r}_{xfd}+\frac{r'_{fd}}{x'_{lfd}}(\psi_{md}^{r}-\psi_{fd}''^{r})]$$

$$\omega_r=-\frac{\omega_b}{2Hp}(T_e-T_m)$$

e'^{r}_{xfd}

(from excitation system)

T_m (from governor)

Fig.6. Synchronous generator standard model.

$$I_{pv}=N_p\left(I_{ph}-I_0\left[\exp\left(\frac{\frac{V_{pv}}{N_s}+\frac{N_C}{N_p}I_{pv}R_s}{aN_CV_{th}}\right)\right.\right.$$

$$\left.\left.-1\right]-\frac{\frac{V_{pv}}{N_s}+\frac{N_C}{N_p}I_{pv}R_s}{N_CR_p}\right) \qquad (1)$$

where I_{pv} and V_{pv} are the current and voltage of the PV array, I_{ph} is the light generated current of the cell, I_0 is diode saturation current, V_{th} is thermal voltage, R_s and R_p are series and parallel resistances, a is diode ideality factor, N_c is the number of cells in module, N_p and N_s are the quantities of PV modules in parallel and series.

C. Wind energy generation

Wind energy is harnessed by wind turbines, which convert it into electrical power. One of the most applied
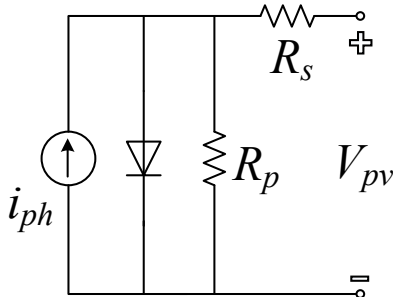

Fig. 7. PV equivalent circuit.

designs is the combination of a wind turbine, gearbox, doubly-fed induction generator (DFIG), harmonic filters, and a back-to-back PWM partial power converter. A block diagram of such a system is presented in Fig. 9.

DFIG is modeled as a wound rotor induction machine with bidirectional power flow in the rotor circuit. The stator circuit is connected directly to the AC grid and supply unidirectional power to the grid. Like the SG, DFIG is presented by the set of differential equations (Fig. 10).

Wind turbine model is represented by the following equation:

$$P_m=c_p(\lambda,\beta)\frac{\rho A}{2}v_{wind}^3 \qquad (2)$$

where P_m is turbine mechanical power, c_p is performance coefficient of the turbine, ρ is air density, A is turbine swept area, the v_{wind} is wind speed, λ,β are tip speed ratio and blade pitch angle.

D. Battery storage system

Battery energy storage system (BESS) is used in the system to extend its flexibility. For higher reliability, the battery can be connected to the grid via a back-to-back DC/AC converter. (Fig. 11.) The battery dynamic model was described and experimentally validated by the authors [17].

The state of charge (SOC) of the battery energy storage system can be expressed in the discrete-time domain as follows:

$$SOC_{(j+1)}=(1-d)SOC_{(j)}-t_s\frac{\eta_{bat}}{E_{nom}}P_{bat(j)}$$

where d is the self-discharging rate; η_{bat} is the charging or discharging efficiency; E_{nom} is the battery nominal energy; $P_{bat(j)}$ is the power flowing from or to the battery at time t_s.
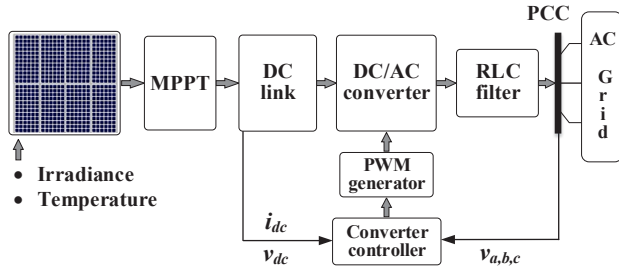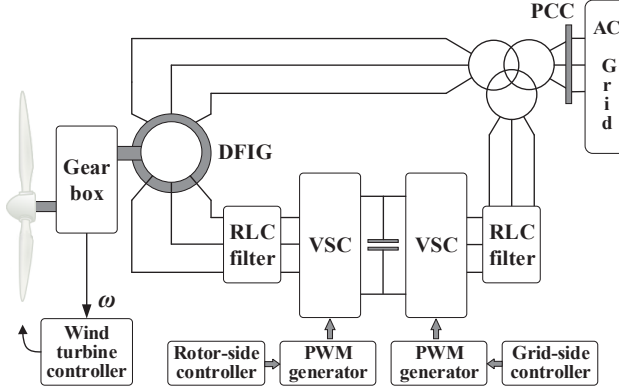
Fig. 8. Grid-connected PV unit.

Fig. 9. Wind energy conversion system.

E. Dump load

Demand-side flexibility measures include the controlled resistive load. It transforms the electric energy into waste heat when combined generated energy exceeds the demand. In a way, the inability to control renewable energy is substituted by controllable demand.

Dump load consists of several three-phase resistors connected in series with power electronic switches. The total overall resistance follows a binary progression and can be adjusted accordingly in a step progression (P_{step}).

F. Low load diesel generator

Low Load Diesel (LLD) allows an engine's full capacity to be utilized by removing the engine's low load limit, 30~40% of the rated capacity as set within the conventional diesel engine.

The lower the diesel generators can run, the larger load can be allocated to RE technologies. LLD requires no new hardware, adopting the existing diesel assets, without modification to the mechanical or electrical architecture. The LLD model is shown in Fig. 13. The value τ1 is the engine delay, which represents combustion delay, the time between the actuator fuel-injection and the production of mechanical torque [18, 19], the power-stroke delay [20], and the ignition delay. In an LLD configuration, the ignition delay is longer compared to a conventional asset due to the lower operating load. With the Watson [21, 22] formulation used to predict the ignition delay, the value for the LLD is 0.3~0.5 ms higher than that for the conventional.

The model of an LLD generator, comprised of a governor, engine and generator is presented in Fig. 13.

Fuel costs for the diesel generator are calculated for a chosen time and expressed by the quadratic cost function as follows:

$$F_g = a_g + b_g P_g + c_g P_g^2$$

where a, b, c are the parameters related to diesel generator fuel consumption; C is the price of one liter of diesel fuel; P_g is the power generated by the diesel unit.

V. CASE STUDIES

Many papers suggest that future electric power system will be mainly driven by RES. However, current large-scale interconnected power systems are still dependent on fossil fuel. High RES penetration is now achieved in many isolated power systems, where small network size and high generation costs justify the means. For IPSs, a single RES integration project results in significant penetration, making them particularly relevant for validating and testing new methods and technologies.

This paper presents a King island IPS as a test case for the developed methodology. The IPS has an average load of 1.5 MW and annual RES penetration around 60%. The system consists of a portfolio of diesel generators, wind turbines, solar arrays, a dump load and a battery energy
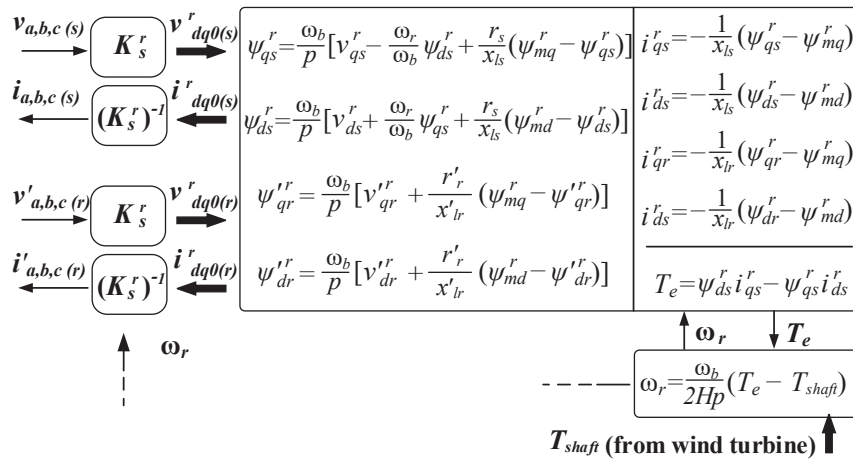

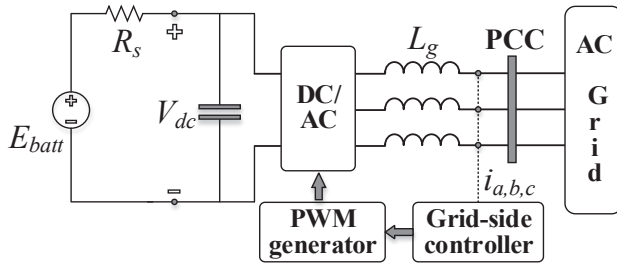*Fig. 10. Doubly-fed induction generator standard model*

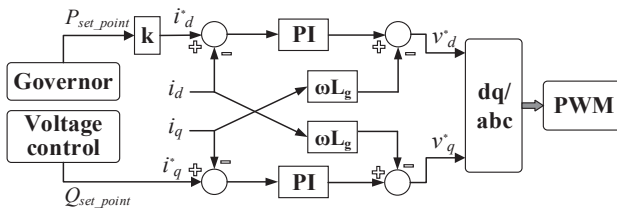**Fig. 11. Doubly-fed induction generator standard model**
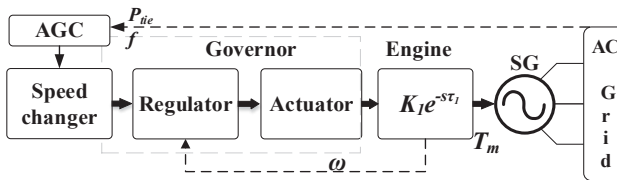

Fig. 12. VOC with a decoupled controller.

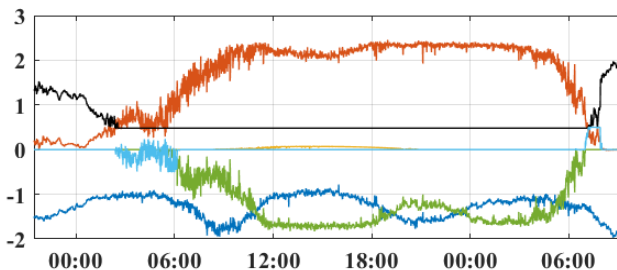**Fig. 13. LLD model.**
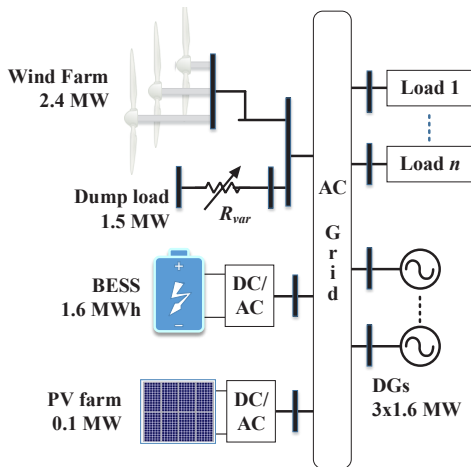
Fig. 14. Island isolated power system.

Table 1. Coefficients for the cost function

Source	a	b	c
Diesel	30	$4e^{-8}$	$6e^{-11}$

Table 2. priority dispatch for re maximization

Element	Priority given excess of generation
Diesel generator	1
Battery	2
Dump load	3

storage system (Fig. 14).

Four RES integration case studies are presented, case study 1 investigates minimal diesel fuel consumption with low capacity battery ESS, while case study 2 considers a high capacity ESS for greater system flexibility allowing prolonged zero-diesel operation (ZDO). Case study 3 looks into the minimization of operating costs by adopting LLD technology, while case study 4 maximizes RES utilization. Table 1 presents a one-year comparison of all four control strategies.

Diesel generator cost function, expressed by the quadratic equation with the coefficient shown in Table 1, represents experimental data obtained in our studies.

The IPS control center sends control action to dispatchable generation and consumption units. In this case, diesel generator, battery ESS and dump load can be adjusted to achieve the desired operational point. When the generation exceeds consumption, the control center operates following the priority dispatch presented in Table 2. Reverse priority is used for the negative system energy mismatch.

A. Control strategy involving low capacity BESS

Case study 1 presents the operation of the system with low capacity BESS. The battery is used to shift renewable energy from periods of favorable weather conditions (from 03:00 to 6:00) to period when only diesel generation is available to cover the load (from 06:00 next day), shown in Fig. 15.

The battery is used to cover any mismatch in the system up until it reaches its critical SOC. When the battery is
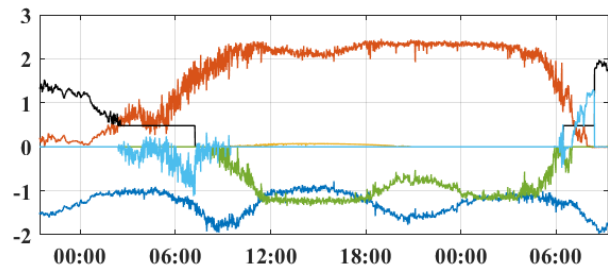

Fig. 15. Case study 1. IPS control strategy involving low capacity BESS. 1 (dark blue line) – power demand, 2 (red line) – wind power, 3 (orange line) – PV power, 4 (black line) – diesel power, 5 (green line) – dump load power, 6(light blue line) – battery power.
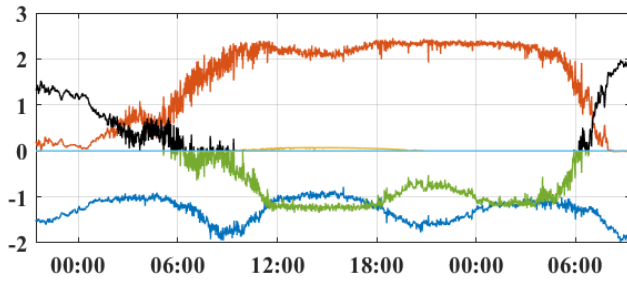

Fig. 16. Case study 2. IPS control strategy involving high capacity BESS. 1 (dark blue line) – power demand, 2 (red line) – wind power, 3 (orange line) – PV power, 4 (black line) – diesel power, 5 (green line) – dump load power, 6 (light blue line) – battery power.

Fig. 17. Case study 3. IPS control strategy involving LLD.
1 (dark blue line) – power demand, 2 (red line) – wind power, 3 (orange line) – PV power, 4 (black line) – diesel power, 5 (green line) – dump load power, 6 (light blue line) – battery power.
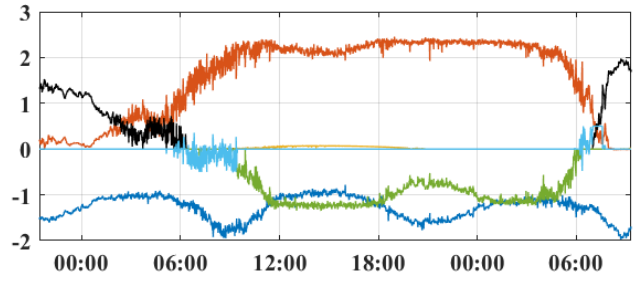

Fig. 18. Case study 4. IPS control strategy involving BESS and LLD.
1 (dark blue line) – power demand, 2 (red line) – wind power, 3 (orange line) – PV power, 4 (black line) – diesel power, 5 (green line) – dump load power, 6 (light blue line) – battery power.

Table 3. Control strategy analysis over one day for case 1.

Allocated energy	Spilled RE	Operating costs
48.2% Diesel energy / 51.8% RE	33.1MWh	Diesel: 138$/MWh

Table 4. control strategy analysis over one day for case 2.

Allocated energy	Spilled RE	Operating costs
22.4% Diesel energy / 77.6% RE	21.1MWh	Diesel: 91.2 $/MWh

Table 5. Control strategy analysis over one day for case 3.

Allocated energy	Spilled RE	Operating cost
22.6% Diesel energy / 77.4% RE	21.3MWh	Diesel: 94 $/MWh

Table 6. Control strategy analysis over one day for case 4.

Allocated energy	Spilled RE	Operational cost
21.5% Diesel energy / 78.5% RE	20.7 MWh	Diesel: 91.6 $/MWh

fully charged, the dump load performs power regulation (from 6:00 to 6:00 next day). It is worthwhile to note that due to insufficient security margin, the conventional diesel generator cannot be disconnected during the considered interval, operating at its low limit (30% of nominal power).

This strategy maximizes renewable energy penetration capturing some energy that would otherwise be wasted by the controlled resistive load.

Table III presents an analysis of the proposed control strategy, where the first column shows the penetration of RES during the considered day, the second column indicates the value of spilled RE. The last column presents the operating costs of a diesel generator. Although the significant RE utilization can be observed (52%), the diesel operating costs are high.

B. Control strategy involving high capacity BESS

According to case study 1, the higher the battery capacity the higher RES penetration can be achieved. An advanced lead-acid battery of 1.6 MWh can supply the entire island with power for up to 45 minutes. Besides, such a battery can improve system flexibility as it operates within the range from -1MW to 1MW. This, in turn, increases the security margin, which allows the ZDO from 08:00 to 8:00, as shown in Fig. 16.

Low-load diesel operating costs and high RES penetration are achieved as shown in Table IV. Although it goes beyond the scope of this paper, it has to be mentioned that with this approach high capital and operating costs associated with battery are inevitable.

C. Control strategy involving LLD

Another approach to high renewable penetration is to increase the flexibility of a generation unit, to allow its operation below 30 %. This results in high RES utilization with lower diesel fuel consumption.
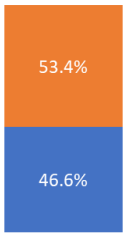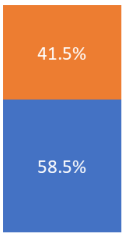
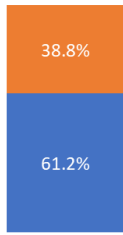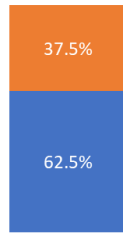As shown in Fig17, the low-load diesel generator is capable to operate from 04:00 to 06:00 on its own releasing the need to trigger either dump load or BESS.

As shown in Table 5, LLD technology adopted by the proposed strategy enables similar RE penetration (77.4% compared to 77.6%) without the need for a storage system.

D. Control strategy involving BESS and LLD

For maximum RES utilization, LLD technology can

Table 7. One-year comparison of control strategies.

	Conventional diesel (0.6 MWh battery)	Conventional diesel (1.6 MWh battery)	LLD (no battery)	LLD (0.6 MWh battery)
RE penetration (%)	46.6	58.5	61.2	62.5
Wasted RE (GWh)	3.44	2.06	1.81	1.63
The operating costs of diesel ($/MWh)	154	131.68	128.3	125.8

be extended by the inexpensive small capacity BESS. As shown in Fig. 18 and Table VI, it extends ZDO at the time interval from 06:00 to 08:00 and allows the shift of RE.

Table 7 demonstrates an annual analysis of the proposed control strategies.

VI CONCLUSION

The control strategies for high renewable penetration in the electric power system were discussed. In addition to greater RES utilization, these strategies were aimed at improving the system flexibility and reliability. The proposed strategies were applied to the case of an isolated power system, comprised of diesel, wind, and PV solar generation. The system was also equipped with a controlled resistive load and a battery energy storage system or low-load diesel generator. It is shown that great RES utilization (around 58,5 % p.a.) can be achieved by using high capacity BESS, which results in low diesel consumption (131.68$/MWh). However, such technology is still young and involves high capital investments. A similar level of penetration and fuel saving was achieved by using LLD technology. For maximum RES penetration (62.5% p.a.), LLD is integrated with low-capacity inexpensive BESS, which additionally results in lower diesel fuel costs (125 $/MWh).

REFERENCES

[1] A. Bloess, W.-P. Schill, and A. Zerrahn, "Power-to-heat for renewable energy integration: A review of technologies, modeling approaches, and flexibility potentials," *Applied Energy*, vol. 212, pp. 1611-1626, 2018/02/15/ 2018.

[2] W. Europe, "Wind in power: 2016 European statistics," Bruksela: *Wind Europe*, 2017.

[3] P. D. Lund, J. Lindgren, J. Mikkola, and J. Salpakari, "Review of energy system flexibility measures to enable high levels of variable renewable electricity," *Renewable and Sustainable Energy Reviews*, vol. 45, pp. 785-807, 2015/05/01/ 2015.

[4] J. P. Deane, B. P. Ó Gallachóir, and E. J. McKeogh, "Techno-economic review of existing and new pumped hydro energy storage plant," *Renewable and Sustainable Energy Reviews*, vol. 14, no. 4, pp. 1293-1302, 2010/05/01/ 2010.

[5] F. Gutiérrez-Martín, D. Confente, and I. Guerra, "Management of variable electricity loads in wind – Hydrogen systems: The case of a Spanish wind farm," *International Journal of Hydrogen Energy*, vol. 35, no. 14, pp. 7329-7336, 2010/07/01/ 2010.

[6] S. Sundararagavan and E. Baker, "Evaluating energy storage technologies for wind power integration," *Solar Energy*, vol. 86, no. 9, pp. 2707-2717, 2012/09/01/ 2012.

[7] X. Tang, X. Hu, N. Li, W. Deng, and G. Zhang, "A Novel Frequency and Voltage Control Method for Islanded Microgrid Based on Multienergy Storages," *IEEE Transactions on Smart Grid*, vol. 7, no. 1, pp. 410-419, 2016.

[8] G. Delille, B. Francois, and G. Malarange, "Dynamic frequency control support by energy storage to reduce the impact of wind and solar generation on isolated power system's inertia," *IEEE Transactions on Sustainable Energy*, vol. 3, no. 4, pp. 931-939, 2012.

[9] M. G. Molina and P. E. Mercado, "Power Flow Stabilization and Control of Microgrid with Wind Generation by Superconducting Magnetic Energy Storage," *IEEE Transactions on Power Electronics*, vol. 26, no. 3, pp. 910-922, 2011.

[10] D. Nikolic and M. Negnevitsky, "Practical Solution for the Low Inertia Problem in High Renewable Penetration Isolated Power Systems," *IEEE Power & Energy Society General Meeting (PESGM)*, 2018, pp. 1-5.

[11] J. Alipoor, Y. Miura, and T. Ise, "Power System Stabilization Using Virtual Synchronous Generator With Alternating Moment of Inertia," *IEEE Journal of Emerging and Selected Topics in Power Electronics*,

vol. 3, no. 2, pp. 451-458, 2015.

[12] M. Dreidy, H. Mokhlis, and S. Mekhilef, "Inertia response and frequency control techniques for renewable energy sources: A review," *Renewable and Sustainable Energy Reviews*, vol. 69, pp. 144-155, 2017/03/01/ 2017.

[13] K. V. Vidyanandan and N. Senroy, "Primary frequency regulation by deloaded wind turbines using variable droop," *IEEE Transactions on Power Systems*, vol. 28, no. 2, pp. 837-846, 2013.

[14] M. A. G. d. Brito, L. Galotto, L. P. Sampaio, G. d. A. e. Melo, and C. A. Canesin, "Evaluation of the Main MPPT Techniques for Photovoltaic Applications," *IEEE Transactions on Industrial Electronics*, vol. 60, no. 3, pp. 1156-1167, 2013.

[15] J. Hamilton, M. Negnevitsky, X. Wang, and S. Lyden, "High penetration renewable generation within Australian isolated and remote power systems," *Energy*, vol. 168, pp. 684-692, 2019.

[16] J. Hamilton, A. Tavakoli, M. Negnevitsky, and X. Wang, "Investigation of no-load diesel technology in isolated power systems," in *Power and Energy Society General Meeting (PESGM)*, pp. 1-5: IEEE, 2016

[17] O. Tremblay and L.-A. Dessaint, "Experimental validation of a battery dynamic model for EV applications," *World electric vehicle journal*, vol. 3, no. 2, pp. 289-298, 2009.

[18] L. Hannett, F. De Mlello, G. Tylinski, and W. Becker, "Validation of nuclear plant auxiliary power supply by test," *IEEE Transactions on Power Apparatus and Systems*, no. 9, pp. 3068-3074, 1982.

[19] K. Yeager and J. Willis, "Modeling of emergency diesel generators in an 800-megawatt nuclear power plant," *IEEE Transactions on Energy Conversion*, vol. 8, no. 3, pp. 433-441, 1993.

[20] R. Morris, H. Hopkins, and R. Borcherts, "An identification approach to throttle-torque modeling," *SAE Technical Paper* 0148-7191, 1981.

[21] N. Watson, A. Pilley, and M. Marzouk, "A combustion correlation for diesel engine simulation," *SAE Technical Paper* 0148-7191, 1980.

[22] D. N. Assanis, Z. S. Filipi, S. B. Fiveland, and M. Syrimis, "A predictive ignition delay correlation under the steady-state and transient operation of a direct injection diesel engine," *Journal of Engineering for Gas Turbines and Power*, vol. 125, no. 2, pp. 450-457, 2003.